LETTER

doi:10.1038/nature11774

ATP-directed capture of bioactive herbal-based medicine on human tRNA synthetase

Huihao Zhou[1], Litao Sun[1], Xiang-Lei Yang[1] & Paul Schimmel[1]

Febrifugine is the active component of the Chinese herb Chang Shan (*Dichroa febrifuga* Lour.)[1,2], which has been used for treating malaria-induced fever for about 2,000 years. Halofuginone (HF), the halogenated derivative of febrifugine, has been tested in clinical trials for potential therapeutic applications in cancer and fibrotic disease[3–6]. Recently, HF was reported to inhibit T_H17 cell differentiation by activating the amino acid response pathway[7], through inhibiting human prolyl-transfer RNA synthetase (ProRS) to cause intracellular accumulation of uncharged tRNA[8,9]. Curiously, inhibition requires the presence of unhydrolysed ATP. Here we report an unusual 2.0 Å structure showing that ATP directly locks onto and orients two parts of HF onto human ProRS, so that one part of HF mimics bound proline and the other mimics the 3′ end of bound tRNA. Thus, HF is a new type of ATP-dependent inhibitor that simultaneously occupies two different substrate binding sites on ProRS. Moreover, our structure indicates a possible similar mechanism of action for febrifugine in malaria treatment. Finally, the elucidation here of a two-site modular targeting activity of HF raises the possibility that substrate-directed capture of similar inhibitors might be a general mechanism that could be applied to other synthetases.

ProRS is a member of the aminoacyl-tRNA synthetase family of enzymes that activate amino acids for protein synthesis through formation of aminoacyl adenylates (AA-AMP) and subsequent transfer of the activated amino acids to the 3′ ends of the cognate tRNAs. Because of their crucial role in protein synthesis, inhibition halts the growth and suppresses the viability of all cell types. Consequently, aminoacyl-tRNA synthetases are attractive targets for discovering types of drugs such as antibiotics and suppressors of cell hyperproliferation[10,11]. Many tRNA synthetase inhibitors mimic AA-AMPs; the AA-AMP mimics directly occupy and block the active site for ATP and amino acid and compete out the substrate ATP. By contrast, ATP was reported to be essential for HF binding to ProRS[8]. This ATP dependence suggests that HF binds to ProRS through a different mechanism and not as a mimetic of Pro-AMP. Thus, understanding how HF inhibits human ProRS is of great interest.

In its simplest description, HF is composed of a hydroxypiperidine ring joined by bridging atoms to a double-ring halogenated 4-quinazolinone (Fig. 1a). To clarify the mechanism of inhibition of HF, we cloned and expressed human ProRS and were able to obtain co-crystals with a non-hydrolysable ATP analogue ((adenosine 5′-(β, γ-imido)triphosphate) (ATP^a)) and HF, which diffracted to 2.0 Å resolution (Supplementary Table 1). The structure was solved by molecular replacement using *Thermus thermophilus* ProRS as template. The asymmetric unit contained two ProRS molecules that formed a homodimer (Fig. 1b), as also seen in gel filtration experiments (data not shown). Each subunit encoded an amino-terminal catalytic domain characteristic of a class II tRNA synthetase, an

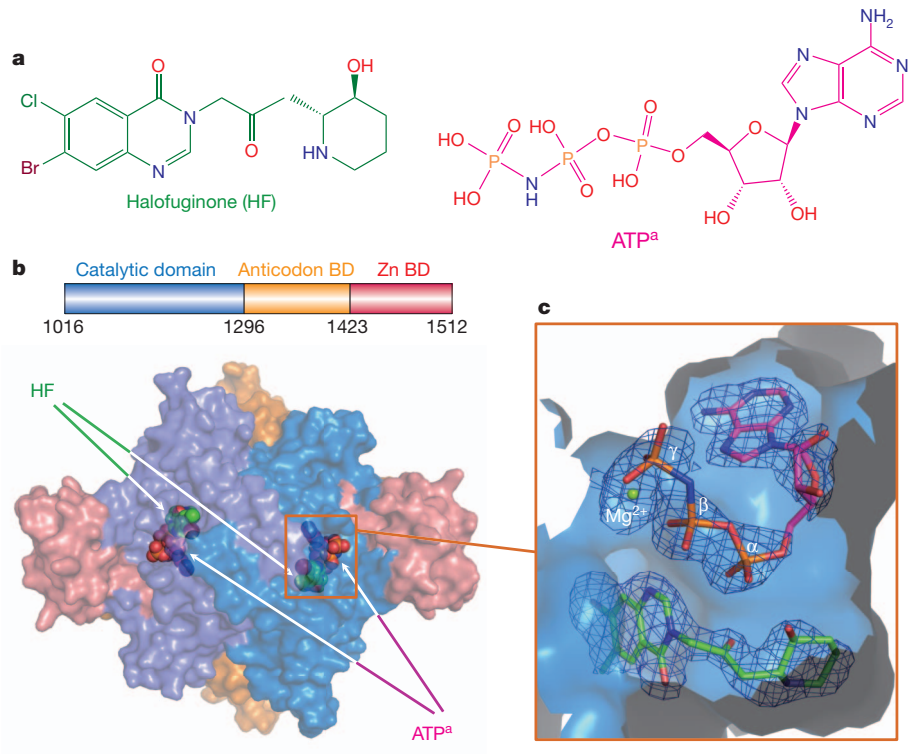

Figure 1 | Structure of human ProRS with bound ligands. **a**, Chemical structures of halofuginone (HF) and the ATP analogue (ATP^a). The colour scheme for HF (green) and ATP^a (red) is the same throughout the manuscript. **b**, Two ProRS monomers form an asymmetric unit that is a homodimer. The domains of ProRS are shown in the colour-coded diagram; BD, binding domain. HF and ATP^a are shown as spherical models at the active site of both subunits. **c**, HF is buried at the bottom of the pocket and covered by co-bound ATP^a. A simulated annealing omit map was calculated with Fourier coefficients $2F_o - F_c$, and contoured at 1.5σ.

[1]The Skaggs Institute for Chemical Biology, Department of Molecular Biology, The Scripps Research Institute, 10550 North Torrey Pines Road, La Jolla, California 92037, USA.

anticodon-binding domain and a carboxy-terminal zinc-binding domain (Fig. 1b). In the two catalytic domains of the ProRS homodimer, HF and ATP[a] were bound to the active site for Pro-AMP formation (Fig. 1b, c).

ATP[a] was located at the canonical ATP-binding pocket of class II aminoacyl-tRNA synthetases[12]. Three hydrogen bonds contributed by Thr 1164 and Thr 1276 and hydrophobic stacking of Phe 1167 stabilized the adenosine group (Supplementary Fig. 2). The ribose moiety was bound by three hydrogen bonds with Gln 1237, Thr 1240 and Arg 1278. The hydrogen bonds from Arg 1152 and Arg 1163 contributed to stabilizing the α-, β- and γ-phosphate groups of ATP[a] (Supplementary Fig. 2), which form a cap over the HF-binding pocket (Fig. 1c). These extensive hydrophilic and hydrophobic interactions positioned the ATP in a 'U'-like bent conformation with the α-phosphate group exposed at the bottom of the U shape. Superposition of the catalytic domains of human ProRS with that of the previously determined structure of *T. thermophilus* ProRS showed that the conformation and location of ATP was the same (Supplementary Fig. 3), with the α- phosphate group poised for proline activation. In the human ProRS–HF–ATP[a] ternary complex, the α-phosphate group is proximal to the hydroxypiperidine ring of HF and forms two hydrogen bonds with its hydroxyl group (Fig. 2a, b). It also forms an additional hydrogen bond with the keto group in the bridge between the piperidine ring and the quinazolinone moiety of HF (Fig. 2a, b). These direct hydrogen-bond interactions may enable ATP to lock onto and orient HF.

In addition to the interactions with ATP, ProRS itself forms seven hydrogen bonds and several hydrophobic contacts with each moiety of HF (Fig. 2a, b). Thus, the pocket for the HF piperidine ring, built by Thr 1121, Glu 1123, Trp 1169, Glu 1171, His 1173, Thr 1240, His 1242 and Ser 1272 (Fig. 2c), has both hydrophobic and hydrophilic character. These residues are highly conserved among eukaryotic ProRS (Supplementary Fig. 4), and were found to be also important for proline recognition in the structure of *T. thermophilus* eukaryotic-like ProRS with proline (Fig. 2d)[13]. Overlay of the catalytic domains of human and *T. thermophilus* ProRS structures showed the piperidine ring of HF bound to the same site as proline (Fig. 2e). In particular, the

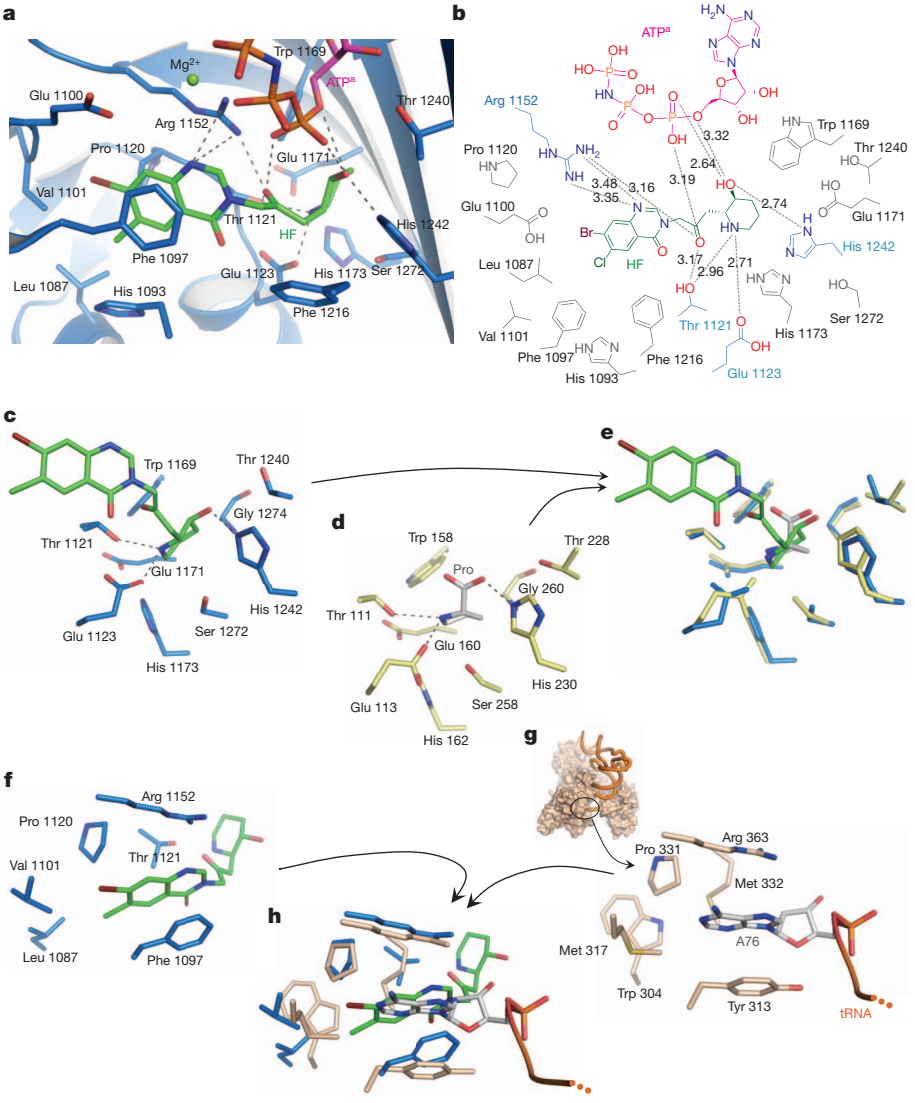

Figure 2 | Mechanistic basis for ATP-dependent inhibition of ProRS by halofuginone. **a**, HF forms extensive hydrophobic contacts and hydrogen-bonding interactions with ProRS and with ATP[a]. **b**, Two-dimensional presentation of HF binding. The HF, ATP[a] and hydrogen-bonded residues are coloured as previously, and other residues within 4 Å of HF are coloured in grey. **c**, A stick model showing the binding of the piperidine ring of HF to human ProRS. **d**, The proline binding pocket of *T. thermophilus* ProRS in complex with proline (Protein Data Bank 1H4T, protein is coloured as yellow and proline as grey-white). **e**, Structure superposition of the catalytic domain of human ProRS with *T. thermophilus* ProRS reveals the piperidine ring of HF directly occupies the proline-binding pocket. **f**, Stick model showing the binding of the halogenated 4-quinazolinone group of HF to human ProRS. **g**, Structure of *E. coli* ThrRS–tRNA complex, with the pocket for the adenosine group for A76 (PDB 1QF6). **h**, Overlay of the catalytic domain of human ProRS onto *E. coli* ThrRS (brown) reveals that HF uses the binding pocket for A76 of the CCA[76] 3′ end for binding the quinazolinone moiety.

orientations of the proline pyrrolidine ring and of the HF piperidine ring, and the locations of nitrogen and oxygen atoms, are similar. Thus, the HF piperidine ring structurally mimics a proline-like group, and would directly compete with proline and block proline activation. The proline mimic mechanism is consistent with the observation that HF or febrifugine derivatives with piperidine ring modifications are unable to bind to the proline-binding pocket and therefore are rendered unable to inhibit or bind to ProRS or affect cell function (for example, MAZ1310 ref. 8). In contrast, derivatives that replaced the piperidine ring by the pyrrolidine ring of proline retained similar or superior biological activity[14].

The halogenated 4-quinazolinone group is buried in a pocket mainly composed of Leu 1087, Phe 1097, Val 1101, Pro 1120, Thr 1121 and Arg 1152 (Fig. 2a, f). In addition to the hydrogen bonds between Arg 1152 and the quinazoline nitrogen atom, the quinazolinone group was mainly stabilized by hydrophobic contacts, particularly by the hydrophobic stack effect from Phe 1097 (Fig. 2a, f). Threonyl-tRNA synthetase (ThrRS) also belongs to class II aminoacyl-tRNA synthetases, and it is most similar to ProRS. Arg 1152 and Phe 1097 of ProRS are conserved in class II synthetases. The corresponding residues Arg 363 and Tyr 313 in the structure of *Escherichia coli* ThrRS were found to flank the two sides of the adenosine A76 of $tRNA^{Thr}$ and thus play crucial roles in CCA 3′-end binding (Fig. 2g)[15]. In addition to these two residues, other parts of the A76 adenosine pocket are also quite similar to the quinazolinone group binding pocket in the ProRS structure (Fig. 2g). Overlay of the ProRS and ThrRS structures by aligning the conserved 7-strand β-sheet core of their catalytic domains showed that the quinazolinone group of HF bound to the same position as bound A76, and with a similar orientation and side-chain contacts (Fig. 2h). This structural similarity indicates that the quinazolinone group of HF binds to ProRS by using a strategy of mimicking the terminal adenosine of the tRNA substrate. Thus, in contrast to the single-site and conventional AA-AMP mimics, HF is a dual-site inhibitor by virtue of simultaneously occupying two active site pockets, the proline binding pocket and the binding pocket for the 3′ end of the tRNA (Supplementary Fig. 1).

We used our crystal structure of the ProRS–ATP–HF complex to further dissect the mechanism of action of HF. Earlier work by other groups showed that HF specifically inhibits overall aminoacylation of $tRNA^{Pro}$ and that binding of HF to ProRS is greatly enhanced by ATP[8] (the level of HF binding, in the absence of ATP, was unknown and presumably weak). According to our structure, HF is 'two-headed' and, with bound ATP, uses the piperidine ring to block the proline binding site and the quinazolinone group to block the site for docking the 3′ end of $tRNA^{Pro}$. We designed experiments to probe the function of each site, the site for adenylate formation/binding and the site for docking the 3′ end of tRNA. In addition to HF, we used another inhibitor, Pro-SA (5′-*O*-(*N*-(L-prolyl)-sulphamoyl-adenosine), as a comparator. Pro-SA is a tight-binding non-reactive adenylate analogue of Pro-AMP[16].

We first determined that the thermal melting of ProRS was barely affected by either proline or ATP^a. In contrast, in the presence of HF the melting curve was shifted to a higher temperature by about 10 °C by HF alone, and by about 18 °C with HF plus ATP^a (Fig. 3a). These data show that HF binds even in the absence of ATP, and also confirm that HF binds much tighter in the presence of ATP. Not surprisingly, the largest thermal shift was obtained with Pro-SA.

To probe the adenylate-formation site, we studied the first step of aminoacylation, which is the activation of proline by ProRS to form a tightly bound Pro-AMP adenylate complex and release of pyrophosphate (PPi). This reaction step is ProRS + Pro + ATP → ProRS–Pro-AMP + PPi.

The conventional proline-dependent ATP–PPi exchange reaction was used to investigate this reaction. As expected, both Pro-SA and HF were potent inhibitors of this reaction in a dose-dependent fashion, with Pro-SA being more effective (Fig. 3b). This result is consistent with the thermal melting data of Fig. 3a showing the tighter binding of Pro-SA, and with our X-ray crystal structure showing the docking of one 'head' of HF at the site for the prolyl moiety of Pro-AMP.

Next, we investigated the ability of HF to mimic the docking of A76 of $tRNA^{Pro}$ to ProRS. For this purpose we studied the effect of HF on the relatively stable preformed ProRS–Pro-AMP complex, isolated using a column. Because binding of tRNA to tRNA synthetases is generally associated with conformational changes that mobilize the active site for transfer of the activated amino acid to A76, we reasoned that binding of the A76-mimicking quinazolinone group of HF would result in an abortive transfer and thereby release Pro-AMP from ProRS. Accordingly, the ProRS–Pro-AMP complex was incubated separately with Pro-SA (which should not have access to the A76 site) and with HF (without ATP). As expected, Pro-SA caused some reduction in the bound Pro-AMP, which is attributed to an exchange on the enzyme between bound Pro-AMP and Pro-SA. In contrast, free HF, while having a much lower affinity than Pro-SA for ProRS, completely released Pro-AMP from the complex (Fig. 3c).This result supports the conclusion (from our X-ray structure) that HF also mimics A76 of tRNA.

HF is a halogenated derivative of febrifugine, which is the bioactive constituent in the Chang Shan herb that has long been used to treat malaria. The ProRS binding sites of both human and the malaria

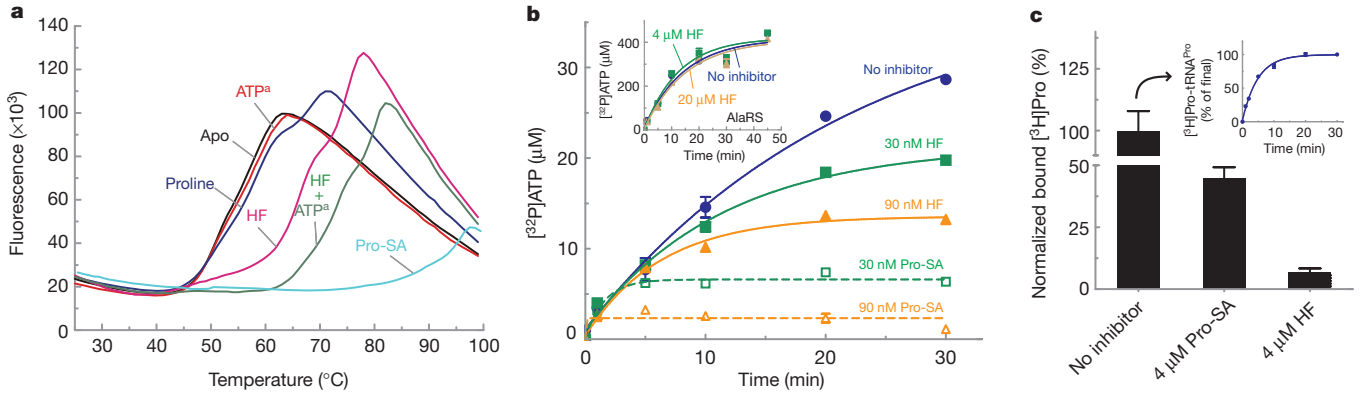

Figure 3 | HF interacts with both the site for amino acid activation and the site for docking the 3′-end of tRNA. **a**, Thermal melting[19] of ProRS in the presence of different ligands. HF binds in the absence of ATP^a, and binds more strongly in the presence of ATP^a. Apo, apoenzyme. Fluorescence units are arbitrary. **b**, HF and the comparator Pro-SA block formation of Pro-AMP, in the proline-dependent ATP–PPi exchange reaction. The inset shows that HF had no effect on the alanine-dependent ATP–PPi exchange reaction with AlaRS. **c**, HF mobilizes the release of Pro-AMP from ProRS. The ProRS–[^{3}H]Pro-AMP complex was prepared on ice and then isolated on a column and for 10 min was left untreated, or exposed to HF, or exposed to Pro-SA, respectively. The complex was then re-run on the column and the amount of bound [^{3}H]Pro-AMP was determined. The inset shows that the isolated [^{3}H]Pro was activated (as [^{3}H]Pro-AMP) and could be transferred to tRNA. Error bars are s.e.m. ($n = 2$).

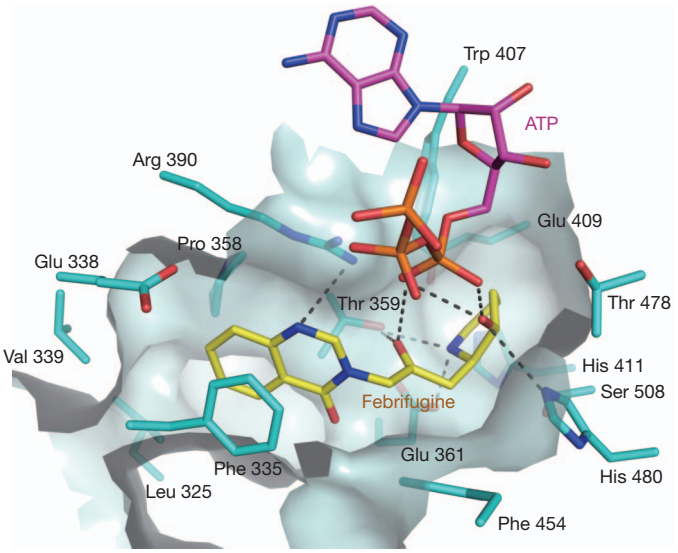

Figure 4 | Febrifugine blocks ProRS. Febrifugine docked to the active site of *P. falciparum* ProRS (UniProtKB code Q8I5R7). ProRS and Febrifugine are coloured cyan and yellow, respectively. The hydrogen bonds are indicated with dashes. The *P. falciparum* ProRS structure was generated by the protein structure homology-modelling server SWISS-MODEL[20]. Febrifugine was docked into the *P. falciparum* ProRS active site based on the structure of ProRS–halofuginone–ATP[a] complex, whereas ATP was docked based on the structure of the *T. thermophilus* ProRS–tRNA–ATP complex (PDB code 1H4Q).

parasite *Plasmodium falciparum* are highly similar (Supplementary Fig. 4). With that in mind, using our ATP-dependent docking of HF to human ProRS as a template, we were able to show the potential for febrifugine docking to *P. falciparum* ProRS (Fig. 4). Thus, our analysis suggests malarial ProRS may also be the target of febrifugine. This possibility could also explain why the lethal effect of febrifugine on *P. falciparum* in culture is reversed by proline[8].

Interestingly, in addition to the inhibition of amino acid activation by mimics of AA-AMP (including the 'operational' mimic pseudomonic acid (mupirocin)[17]), the ATP-dependent two-site HF inhibition mechanism reported here, and the single-site tRNA-dependent editing-site-trapping mechanism reported earlier[18], illustrate two entirely different and unusual mechanisms for substrate participation in capture of an inhibitor (Supplementary Fig. 5). In addition, by substitution of the piperidine ring with other amino acid mimics, dual-site inhibitors could in principle be designed for other aminoacyl-tRNA synthetases.

METHODS SUMMARY

Human ProRS was overexpressed in *E. coli* and purified by fast protein liquid chromatography. The protein–ligand complex was generated by mixing the protein with 3 mM halofuginone, 5 mM ATP analogue adenosine 5′-(β,γ-imido)triphosphate, 5 mM $MgCl_2$ and 5 mM β-mercaptoethanol. Crystals were obtained by the sitting-drop vapour-diffusion method, and diffraction data were collected using a single flash-frozen crystal. The ProRS–ligand complex structure was determined by the molecular replacement method, using the structure of *T. thermophilus* ProRS (PDB code 1HC7) as the searching model. Standard refinement procedures were performed to get the final model. The ATP-pyrophosphate exchange was as described[21] and the ProRS–Pro-AMP complex was isolated with a desalting column. Results were analysed with GraphPad Prism software.

Full Methods and any associated references are available in the online version of the paper.

Received 15 June; accepted 9 November 2012.
Published online 23 December 2012.

1. Koepfli, J. B., Mead, J. F. & Brockman, J. A. Jr. An alkaloid with high antimalarial activity from *Dichroa febrifuga*. *J. Am. Chem. Soc.* **69,** 1837 (1947).
2. Coatney, G. R., Cooper, W. C., Culwell, W. B., White, W. C. & Imboden, C. A. Jr. Studies in human malaria. XXV. Trial of febrifugine, an alkaloid obtained from *Dichroa febrifuga* Lour., against the Chesson strain of *Plasmodium vivax*. *J. Natl. Malar. Soc.* **9,** 183–186 (1950).
3. Pines, M., Snyder, D., Yarkoni, S. & Nagler, A. Halofuginone to treat fibrosis in chronic graft-versus-host disease and scleroderma. *Biol. Blood Marrow Transplant.* **9,** 417–425 (2003).
4. Pines, M. & Nagler, A. Halofuginone: a novel antifibrotic therapy. *Gen. Pharmacol.* **30,** 445–450 (1998).
5. de Jonge, M. J. *et al.* Phase I and pharmacokinetic study of halofuginone, an oral quinazolinone derivative in patients with advanced solid tumours. *Eur. J. Cancer* **42,** 1768–1774 (2006).
6. Koon, H. B. *et al.* Phase II AIDS Malignancy Consortium trial of topical halofuginone in AIDS-related Kaposi sarcoma. *J. Acquir. Immune Defic. Syndr.* **56,** 64–68 (2011).
7. Sundrud, M. S. *et al.* Halofuginone inhibits T_H17 cell differentiation by activating the amino acid starvation response. *Science* **324,** 1334–1338 (2009).
8. Keller, T. L. *et al.* Halofuginone and other febrifugine derivatives inhibit prolyl-tRNA synthetase. *Nature Chem. Biol.* **8,** 311–317 (2012).
9. Kilberg, M. S., Pan, Y. X., Chen, H. & Leung-Pineda, V. Nutritional control of gene expression: how mammalian cells respond to amino acid limitation. *Annu. Rev. Nutr.* **25,** 59–85 (2005).
10. Schimmel, P., Tao, J. & Hill, J. Aminoacyl tRNA synthetases as targets for new anti-infectives. *FASEB J.* **12,** 1599–1609 (1998).
11. Hill, J. Aminoacyl sulfamides for the treatment of hyperproliferative disorders. US Patent 5,824 657 (1998).
12. Carter, C. W. Jr. Cognition, mechanism, and evolutionary relationships in aminoacyl-tRNA synthetases. *Annu. Rev. Biochem.* **62,** 715–748 (1993).
13. Yaremchuk, A., Tukalo, M., Grotli, M. & Cusack, S. A succession of substrate induced conformational changes ensures the amino acid specificity of *Thermus thermophilus* prolyl-tRNA synthetase: comparison with histidyl-tRNA synthetase. *J. Mol. Biol.* **309,** 989–1002 (2001).
14. Zhu, S. *et al.* Synthesis and biological evaluation of febrifugine analogues as potential antimalarial agents. *Bioorg. Med. Chem.* **17,** 4496–4502 (2009).
15. Sankaranarayanan, R. *et al.* The structure of threonyl-tRNA synthetase-$tRNA^{Thr}$ complex enlightens its repressor activity and reveals an essential zinc ion in the active site. *Cell* **97,** 371–381 (1999).
16. Heacock, D., Forsyth, C. J., Shiba, K. & Musier-Forsyth, K. Synthesis and aminoacyl-tRNA synthetase inhibitory activity of prolyl adenylate analogs. *Bioorg. Chem.* **24,** 273–289 (1996).
17. Nakama, T., Nureki, O. & Yokoyama, S. Structural basis for the recognition of isoleucyl-adenylate and an antibiotic, mupirocin, by isoleucyl-tRNA synthetase. *J. Biol. Chem.* **276,** 47387–47393 (2001).
18. Rock, F. L. *et al.* An antifungal agent inhibits an aminoacyl-tRNA synthetase by trapping tRNA in the editing site. *Science* **316,** 1759–1761 (2007).
19. Pantoliano, M. W. *et al.* High-density miniaturized thermal shift assays as general strategy for drug discovery. *J. Biomol. Screen.* **6,** 429–440 (2001).
20. Arnold, K., Bordoli, L., Kopp, J. & Schwede, T. The SWISS-MODEL workspace: a web-based environment for protein structure homology modeling. *Bioinformatics* **22,** 195–201 (2006).
21. Beebe, K. *et al.* A universal plate format for increased throughput of assays that monitor multiple aminoacyl transfer RNA synthetase activities. *Anal. Biochem.* **368,** 111–121 (2007).

Supplementary Information is available in the online version of the paper.

Acknowledgements We thank K. Musier-Forsyth for providing the ProRS gene plasmid and Pro-SA, staff at beamline 7-1 of Stanford Synchrotron Radiation Lightsource for assistance in X-ray diffraction data collection, and M. Guo for comments. This work was supported by National Institutes of Health grants GM15539, GM23562 and GM88278 and by a fellowship from the National Foundation for Cancer Research.

Author Contributions H.Z., L.S., X.-L.Y. and P.S. designed the experiments. H.Z. and L.S. performed the experiments and all authors analysed the data. All authors discussed the results and H.Z. and P.S. wrote the manuscript.

Author Information Atomic coordinates and structure factors for the reported crystal structure have been deposited in the Protein Data Bank under accession code 4HVC. Reprints and permissions information is available at www.nature.com/reprints. The authors declare no competing financial interests. Readers are welcome to comment on the online version of the paper. Correspondence and requests for materials should be addressed to P.S. (schimmel@scripps.edu).

METHODS

Protein expression and purification. The cDNA fragment encoding human prolyl-tRNA synthetase (ProRS) was cloned into *E. coli* plasmid pET21a (Novagen), with an additional N-terminal His_6 tag. The plasmid encoding ProRS was transformed into *E. coli* strain BL21(DE3) pLysS (Life Technologies) and was induced overnight for overexpression with 0.5 mM isopropyl-β-D-thiogalactoside (IPTG) at room temperature. The *E. coli* cell lysate was first loaded onto a nickel–nitrilotriacetic (Ni–NTA) column (Qiagen), and the elution fraction was further purified with mono Q ion-exchange chromatography (GE Healthcare) to a single band as indicated on SDS–polyacrylamide gel electrophoresis with Coomassie brilliant blue staining. The purified protein was found as a single peak with the elution volume consistent with a homogeneous ProRS homodimer on the Superdex 200 analytical gel filtration column (GE Healthcare). The purified ProRS was concentrated to 50 mg ml^{-1} and stored at −80 °C in a buffer of 50 mM NaCl, 2 mM Tris buffer, pH 8.0.

Crystallization and data collection. ProRS was crystallized with the sitting-drop vapour-diffusion method using a Mosquito robot (TTP Labtech). Prior to crystallization, ProRS was diluted to 40 mg ml^{-1} with 3 mM halofuginone (HF) (Sigma-Aldrich), 5 mM ATP analogue adenosine 5′-(β,γ-imido)triphosphate (Sigma-Aldrich), 5 mM $MgCl_2$ and 5 mM β-mercaptoethanol, and then incubated on ice for 30 min. Next, sitting drops were set up by mixing 100 nl of protein (40 mg ml^{-1}) and 100 nl of reservoir solution containing 20% (w/v) polyethylene glycol 3350, 0.6 M $CaCl_2$ and 50 mM HEPES, pH 7.5, and equilibrated against a 70 μl of reservoir solution at 30 °C for 2 to 3 days before data collection. The X-ray diffraction data were collected using a single crystal at 1.000 Å (0.1000 nm) and temperature of 100 K at beamline 7-1 of Stanford Synchrotron Radiation Lightsource. The complete data set contains 500 images with the oscillation angle of 0.5° for each image. The ProRS–HF–ATP[a] crystal belonged to space group $P2_1$. Data were integrated and scaled with the program HKL2000 (ref. 22).

Structure determination and refinement. The initial model was determined by molecular replacement using the program MOLREP[23]. The crystal structure of *T. thermophilus* ProRS (PDB code 1HC7), which has 43% amino acid sequence identity to human ProRS, was used as the searching model. The structure was further refined by iterative cycles of positional refinement and translation-libration-screw refinement with Refmac5[24] and Phenix[25] and model building with COOT[26], and the final model was refined to 2.0 Å resolution with R_{work}/R_{free} of 20.4%/22.7%. The model has good geometry quality, and 98.9%/99.8% residues are in favoured or allowed regions of the MolProbity[27] Ramachandran plot. Statistics of data collection and structure refinement are given in Supplementary Table 1. The atomic coordinates and structural factors have been deposited into Protein Data Bank under the accession code 4HVC.

Sequence analysis and structure presentation. Protein sequences were aligned using the program Multalin[28]. The alignment result was submitted to ESPript[29] for figure generation. All protein structure illustrations were prepared with the program PyMOL (http://www.pymol.org).

Thermal shift assay. ProRS (3 μg) was diluted in 30 μl buffer containing 500 mM NaCl, 20 mM Tris, pH 8.0, 1 to 2,500 dilution SYPRO orange dye (Life Technologies) and different ligands (5 mM ATP[a], 5 mM proline, 1 mM HF, 1 mM HF plus 5 mM ATP[a] or 1 mM Pro-SA, respectively), and incubated at room temperature for 10 min. Then ProRS samples were heated from 25 °C to 98 °C at a rate of 1 °C min^{-1}, and the fluorescence signals were monitored by the StepOnePlus quantitative real-time PCR system (Life Technologies). Each curve was an average of three measurements.

ATP–pyrophosphate exchange assays. The ATP-pyrophosphate exchange was as described[21]. The reaction buffer contained 100 mM HEPES, pH 7.5, 20 mM KCl, 10 mM $MgCl_2$, 1 mM dithiothreitol, 2 mM ATP, 1 mM Na pyrophosphate (NaPPi), 20 μCi ml^{-1} [^{32}P]PP_i and 0.5 mM proline. Inhibitor HF and Pro-SA (5′-*O*-(*N*-(L-prolyl)-sulphamoyl)adenosine (gift of K. Musier-Forsyth) were added at different concentrations (0, 30 or 90 nM). The reactions were started by adding ProRS into buffer at the final ProRS concentration of 10 nM, and then incubated at 20 °C. 20 μl of each of the reactions was quenched at different time points in 200 μl of quench buffer (1 M HCl, 200 mM NaPPi and 4% charcoal). The free [^{32}P]PP_i was removed by flowing through the 96-well polyvinylidene fluoride (PVDF) filter plates, and the residual [^{32}P]PP_i was washed five times using 200 μl of washing buffer (1 M HCl and 200 mM NaPPi). Then the produced [^{32}P]ATP remaining in filter plates was transferred to scintillation vials and counted. The data were analysed with GraphPad Prism (GraphPad Software). The experiments here and following subsequently were independently repeated three times with duplicated measurements each time.

HF–Pro-AMP competition assay. The isolation of ProRS–Pro-AMP was slightly modified from that of a previous report[30]. In brief, 2 μM ProRS was added to the buffer containing 50 mM HEPES, pH 7.5, 20 mM KCl, 5 mM $MgCl_2$, 2 mM ATP, 2 mM dithiothreitol, 20 μM proline and 1 μM [^{3}H]proline, and then incubated at 4 °C for 10 min to create ProRS–[^{3}H]Pro-AMP. The reaction containing ProRS–[^{3}H]Pro-AMP flowed through a desalting column (SpinTrap G-25, GE Healthcare) to isolate the complex and remove the extra ATP and proline. HF and Pro-SA were added at the concentration of 4 μM to the complex to compete for 10 min at 20 °C. The reaction was passed through a desalting column again to remove dissociated [^{3}H]Pro-AMP. The eluted [^{3}H]Pro-AMP still bound to ProRS was then measured.

22. Otwinowski, Z. & Minor, W. Processing of X-ray diffraction data collected in oscillation mode. *Methods Enzymol.* **276,** 307–326 (1997).
23. Vagin, A. & Teplyakov, A. MOLREP: an automated program for molecular replacement. *J. Appl. Crystallogr.* **30,** 1022–1025 (1997).
24. Murshudov, G. N., Vagin, A. A. & Dodson, E. J. Refinement of macromolecular structures by the maximum-likelihood method. *Acta Crystallogr. D* **53,** 240–255 (1997).
25. Adams, P. D. *et al.* PHENIX: a comprehensive Python-based system for macromolecular structure solution. *Acta Crystallogr. D* **66,** 213–221 (2010).
26. Emsley, P. & Cowtan, K. Coot: model-building tools for molecular graphics. *Acta Crystallogr. D* **60,** 2126–2132 (2004).
27. Chen, V. B. *et al.* MolProbity: all-atom structure validation for macromolecular crystallography. *Acta Crystallogr. D* **66,** 12–21 (2010).
28. Corpet, F. Multiple sequence alignment with hierarchical clustering. *Nucleic Acids Res.* **16,** 10881–10890 (1988).
29. Gouet, P., Courcelle, E., Stuart, D. I. & Metoz, F. ESPript: analysis of multiple sequence alignments in PostScript. *Bioinformatics* **15,** 305–308 (1999).
30. Shi, J. P. & Schimmel, P. Aminoacylation of alanine minihelices. 'Discriminator' base modulates transition state of single turnover reaction. *J. Biol. Chem.* **266,** 2705–2708 (1991).